Journal of Applied Sciences and Nanotechnology

Journal homepage: jasn.uotechnology.edu.iq

Microstructure-Modulated Antibacterial Performance of Chemically Precipitated SnO_2 Nanoparticles

[1]Shatha Sh. Batros, [1]Mohammed H. Ali, [1]Ali J. Addie*

[1]Center of Advanced Materials, Materials Research Directorate, Ministry of Science and Technology – Iraq

A R T I C L E I N F O

Article history:
Received: September, 05, 2023
Accepted: October, 20, 2023
Available online: December, 10, 2023

Keywords:
Tin oxide nanoparticles,
Antibacterial activity,
Chemical Precipitation,
Crystallite size control

Corresponding Author:
Ali J. Addie
ali.jaddie@yahoo.com

A B S T R A C T

Tin oxide (SnO_2) nanoparticles were synthesized via a facile chemical precipitation route using tin chloride ($SnCl_2$•$2H_2O$) as precursor and ammonia as precipitant. The as-synthesized nanoparticles were subjected to post-calcination at 300°C, 400°C and 500°C and thoroughly characterized by advanced techniques including X-ray diffraction (XRD), scanning electron microscopy (SEM), energy dispersive x-ray spectroscopy (EDS) and Fourier transform infrared (FTIR) spectroscopy. XRD patterns revealed the formation of a tetragonal SnO_2 crystalline phase with average crystallite sizes of 11.9 nm, 13.9 nm, and 17.2 nm for the samples calcined at 300°C, 400°C and 500°C respectively. SEM micrographs demonstrated agglomerated and irregular morphology of the calcined SnO_2 nanoparticles. FTIR spectra confirmed the presence of characteristic Sn-O and O-Sn-O vibrational modes in the calcined SnO_2 samples. The antibacterial activity of the synthesized nanoparticles was evaluated against model Gram-negative (*Escherichia coli*) and Gram-positive (*Staphylococcus aureus*) bacterial strains by standard zone of inhibition assays. The SnO_2 nanoparticles exhibited excellent antibacterial activity due to their high specific surface area. A systematic increase in the inhibition zone diameter was observed with a decrease in the crystallite size of SnO_2 for both bacterial strains, suggesting an inverse relationship between crystallite size and antibacterial behaviour. The present work demonstrates a simple, eco-friendly synthesis of antibacterial SnO_2 nanoparticles with controlled crystallite size by tuning the calcination temperature.

https://doi.org/10.53293/jasn.2023.7107.1246, Department of Applied Sciences, University of Technology - Iraq.

1. Introduction

Tin oxide (SnO_2) nanoparticles have attracted considerable research interest in recent years owing to their versatile applications in gas sensing, optoelectronics, dye-based solar cells, photocatalysis, antibacterial agents, and other areas [1–4]. SnO_2 is an important n-type wide bandgap (Eg ~3.6 eV) semiconductor metal oxide characterized by its tetragonal rutile structure, excellent chemical stability, thermal stability up to 1100°C in air, high electron mobility, and good optical transparency in the visible region [5–8]. The nanoparticle size, morphology, crystallinity, and surface characteristics strongly influence these remarkable properties. Therefore, controlled synthesis of SnO_2 nanoparticles with tailored structural and optical properties is vital to exploit their full

applications across diverse technological fields. A variety of physical and chemical methods have been developed to synthesize SnO_2 nanoparticles, including thermal evaporation [9], sol-gel [10], hydrothermal [11], microwave irradiation [12], chemical precipitation [13], electrochemical routes [14], etc. However, many of these techniques involve using toxic and hazardous chemicals and high temperatures or high-pressure conditions. There is a need for facile, eco-friendly green chemistry approaches to produce high-quality SnO_2 nanomaterials under ambient conditions. Wet chemical techniques like precipitation are attractive due to their simplicity, low cost, and easy scaled up synthesis without sophisticated instrumentation [12, 15, 16]. Tin (II) oxide (SnO) is a useful precursor for controlled conversion to SnO_2 nanoparticles, but its growth is challenging since Sn^{2+} tends to be oxidized to Sn^{4+} in the air [17]. The morphological features, including particle size, shape, porosity and crystallite size, bandgap, and surface defects, can be effectively tailored by tuning key synthesis parameters such as pH, ageing time, temperature, etc [18, 19]. Calcination of the as-prepared SnO_2 precursor is commonly performed to improve the crystallinity and remove residual organics or moisture. The calcination temperature significantly influences the nanoparticle morphology and crystallite growth [15, 20]. Inorganic nanomaterials exhibit higher thermal and chemical stability than organic antibiotics, making metal oxide nanoparticles such as SnO2 attractive antibacterial agents [15, 18, 21–23]. The antibacterial activity arises from generating reactive oxygen species on the nanoparticle surface and interacting with the cell membrane. The activity depends on the bacterial strain owing to differences in cell wall structure between Gram-positive and Gram-negative species [22,24]. Gram-positive bacteria have a thick peptidoglycan layer containing teichoic and lipoteichoic acids. In contrast, Gram-negative bacteria possess a thin peptidoglycan layer and an outer membrane containing lipopolysaccharides and membrane proteins. There is considerable interest in applying SnO_2 nanoparticles as antibacterial agents against both pathogenic strains [17, 20]. However, systematic studies directly correlating the SnO_2 crystallite size, nanoparticle microstructure and surface defects with the antibacterial behaviour are still lacking. Despite the tremendous potential of SnO_2 nanoparticles as antibacterial agents, most prior works have utilized SnO_2 synthesized using toxic chemicals and harsh conditions [25–27]. Some biochemical techniques have been reported for SnO_2 synthesis but face challenges for scaled-up production [28, 29]. Furthermore, systematic correlations elucidating the dependence of antibacterial activity on the SnO_2 crystallite size, nanoparticle morphology, and surface defects are lacking. Hence, there is an urgent need to develop green chemistry approaches for controlled SnO_2 nanoparticle synthesis and establish structure-property relationships guiding their antibacterial applications [30, 31]. In this work, we seek to address this need for green synthesis and structure-property understanding of SnO_2 nanoparticles by developing an eco-friendly chemical precipitation route for tailored nanoparticle synthesis at room temperature. We utilize tin (II) chloride and ammonia precursors to synthesize SnO_2 nanoparticles with controlled crystallite size, phase purity, and surface defects by adjusting the precursor ratios and post-calcination temperatures. Additionally, we aim to provide new insights into the dependence of reactive oxygen species generation and antibacterial activity on the SnO_2 crystallite size and surface defects against model Escherichia coli and Staphylococcus aureus strains. The SnO_2 nanoparticles are thoroughly characterized by powder X-ray diffraction (XRD), Fourier transform infrared spectroscopy (FTIR), scanning electron microscopy (SEM), and energy dispersive x-ray spectroscopy (EDS) techniques. Furthermore, the antibacterial activity was evaluated against model Gram-negative *Escherichia coli* (*E. coli*) and Gram-positive *Staphylococcus aureus* (*S. aureus*) strains by standard zone of inhibition studies. This synthesis approach and correlation study provide a useful foundation for the potential integration of green synthesized SnO_2 nanomaterials in water treatment and food packaging applications needing targeted antibacterial function.

2. Experimental

2.1 Materials

Tin (II) chloride dihydrate ($SnCl_2 \cdot 2H_2O$, 99.9% purity) and ammonium hydroxide (NH_4OH, 25% in H_2O) were procured from Sigma-Aldrich. Nutrient agar and Mueller-Hinton agar/broth were obtained from HiMedia Laboratories for antibacterial tests. All chemicals were of analytical grade and used as received without further purification.

2.2 Synthesis of SnO_2 Nanoparticles

SnO_2 nanoparticles were synthesized by a facile chemical precipitation method at room temperature. In a typical procedure, 0.1 M aqueous solution of $SnCl_2 \cdot 2H_2O$ precursor was prepared by dissolving 1.89 g of tin (II) chloride dihydrate in 100 mL of deionized water under constant stirring. Ammonium hydroxide was added dropwise to the

salt solution until pH 10 to generate white precipitates of tin hydroxide. The precipitate was aged for 30 min under continuous stirring, filtered, and washed thoroughly with deionized water 3-4 times. The filtered residue was dried overnight at 100°C in a hot air oven to remove moisture. Finally, the dried precursor was calcined at 300°C, 400°C and 500°C for 1 h each in ambient air to obtain pure tetragonal SnO_2 nanoparticles.

2.3 Characterization

The crystallinity and phase purity of the as-synthesized and calcined SnO_2 nanoparticles were examined by X-ray diffraction (XRD, Shimadzu X6000 diffractometer) using CuKα radiation (λ=1.5418 Å). The XRD patterns were recorded at 40 kV and 30 mA over a 2θ range of 20°-80° at a scan rate of 2°/min. The average crystallite sizes were estimated using the Scherrer equation. The surface morphology was studied by scanning electron microscopy (SEM, VegaIII TESCAN). Fourier analyzed the chemical bonding and vibrational modes transform infrared spectroscopy (FTIR, Bruker Alpha II) over 400-4000 cm^{-1} range at 4 cm^{-1} resolutions.

2.4 Antibacterial Testing

The antibacterial activity of the calcined SnO_2 nanoparticles was evaluated against Gram-negative *E. coli* and Gram-positive *S. aureus* by a standard zone of inhibition method using Mueller-Hinton agar medium. Both bacterial strains were grown in Mueller-Hinton broth at 37°C for 17-19 h. The inhibition zone diameters were measured to determine the activity.

3. Results and Discussion

3.1 Structural Characterization

The phase evolution and crystallinity of the as-synthesized and calcined SnO_2 nanoparticles were investigated by powder X-ray diffraction (XRD) measurements using CuKα radiation (λ = 1.5418 Å). Before calcination, the XRD pattern of the precursor sample heated to 100°C showed the formation of an intermediate greyish beige coloured hydro-tin oxide ($Sn_3O_2(OH)_2$) phase as the major component along with minor peaks corresponding to SnO and residual unreacted $SnCl_2{\cdot}2H_2O$ impurities (Fig. 1). The broad overlapped peaks indicate the partially hydrolyzed nature of the as-prepared sample. The minor reflections at 2θ values of 33.3°, 50.7°, 62.5°, and 67.7° can be indexed to the (110), (112), (103) and (113) planes of tetragonal SnO (ICDD #06-0395). This indicates partial hydrolysis of the tin chloride precursor upon adding ammonia to form the oxyhydroxide intermediate. The emergence of hydro-tin oxide ($Sn_3O_2(OH)_2$) as the predominant phase confirms partial hydrolysis of the $SnCl_2{\cdot}2H_2O$ precursor has occurred following ammonia addition, leading to the formation of the oxyhydroxide intermediate. The minor presence of residual $SnCl_2{\cdot}2H_2O$ and SnO indicates the hydrolysis reaction is incomplete at 100°C. This demonstrates that the as-prepared precursor consists of poorly crystalline Sn3O2(OH)2 and traces of unreacted starting materials. Subsequent calcination is necessary to obtain phase pure tetragonal SnO_2, as corroborated by the XRD patterns at higher temperatures. Observing minor $SnCl_2{\cdot}2H_2O$ and SnO impurities provides insights into the reaction kinetics and hydrolysis pathway involved in the low-temperature synthesis. Upon calcination from 300°C to 500°C, the XRD patterns confirmed a successful phase transition to tetragonal rutile SnO_2 as the major phase (ICDD # 41-1445) along with significant improvement in crystallinity. No unidentified impurity peaks were observed, suggesting high phase purity of the calcined SnO_2 nanoparticles. The prominent (110), (101) and (211) reflections correspond to the tetragonal SnO_2 phase. The average crystallite size (D) was estimated from the XRD peak broadening using the Scherrer equation Eq. (1) [32]:

$$D = 0.9\lambda/\beta\cos\theta \quad (1)$$

Where λ is the X-ray wavelength, β is the full width at half maximum (FWHM) of the diffraction peak, and θ is the Bragg angle.

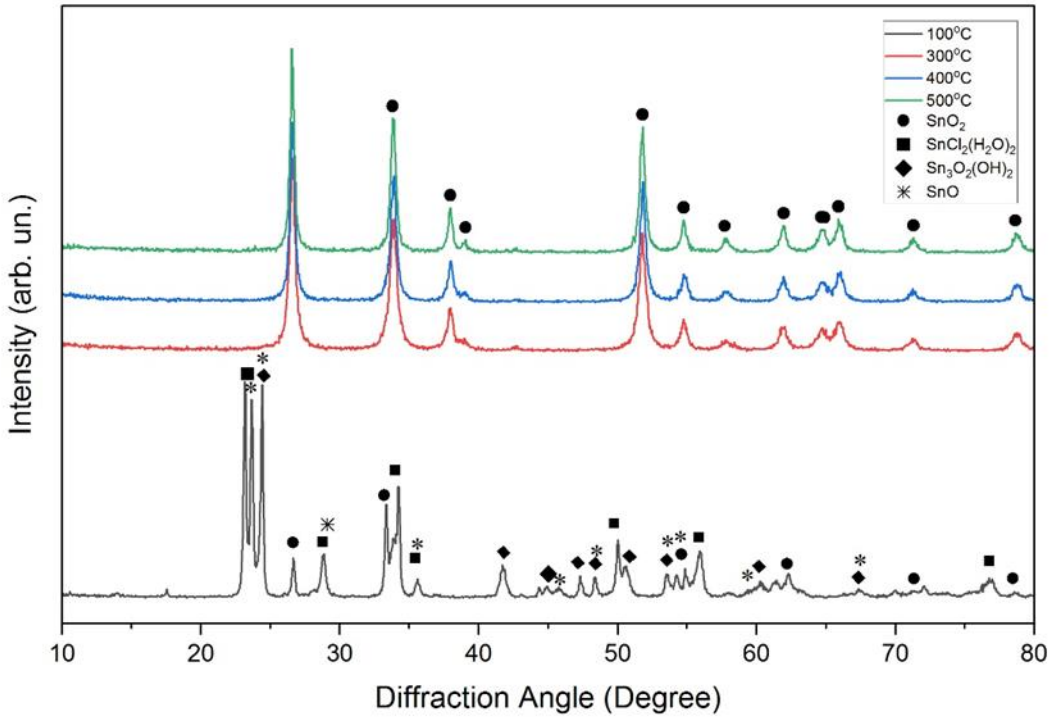

Figure 1: Evolution of SnO_2 phase purity with calcination temperature. XRD precursor pattern at 100°C shows $SnCl_2$•$2H_2O$, $Sn_3O_2(OH)_2$ and SnO phases. Calcined SnO_2 at 300°C, 400°C and 500°C exhibits tetragonal SnO_2 as dominant phase.

The peak breadth decreased progressively with increasing calcination temperature from 300°C to 500°C, indicating crystallite growth. Correspondingly, the crystallite size increased from 11.9 nm to 13.9 nm and 17.2 nm for the samples calcined at 300°C, 400°C and 500°C, respectively, as summarized in Table 1. The particle growth is likely due to aggregation and sintering effects at higher temperatures. Additionally, the enhanced intensity and reduced FWHM of the XRD peaks point to improved crystallinity at higher calcination temperatures owing to the increased ordering of the atomic planes and conversion of amorphous fractions to crystalline SnO_2 phase. The average lattice parameters calculated using the (hkl) plane spacing (d) were determined to be a = b = 4.732 Å and c = 3.660 Å, consistent with tetragonal SnO_2. The XRD analysis confirmed that purity tetragonal SnO2 nanoparticles were obtained after thermal calcination with systematic crystallite growth at higher temperatures.

Table 1: Variation in crystallite size of SnO_2 nanoparticles with calcination temperature estimated from XRD data using Scherrer equation.

Calcination Temperature (°C)	2Theta (deg)	d (Å)	FWHM (deg)	(hkl)	Crystallite Size (nm)
	26.608	3.347	0.489	110	13.01
300	33.864	2.645	0.602	101	10.79
	51.765	1.765	0.575	211	12.01
	26.615	3.347	0.437	110	13..03
400	33.874	2.644	0.480	101	13.53
	51.774	1.764	0.467	211	14.78
	26.593	3.349	0.348	110	18.35
500	33.858	2.645	0.418	101	15.54
	51.764	1.765	0.389	211	17.76

The evolution of surface morphology and microstructure of the as-synthesized and thermally annealed SnO_2 nanopowder were thoroughly investigated using scanning electron microscopy (SEM). Significant changes in

particle morphology and microstructure were observed in the SEM micrographs after calcination from 300°C to 500°C (Fig. 2). At 300°C, partial fusion of nanoparticles into larger irregular clusters occurred leading to surface smoothening, indicative of initial sintering. The average particle size increased to ~68 nm. Further, the rise in calcination temperature to 400°C showed increased densification and grain growth, as evidenced by larger nanoparticles of ~87 nm and distinct grain boundaries. Well-defined facets and polyhedral morphologies were observed in the 500°C calcined sample with an average particle size of ~93 nm.

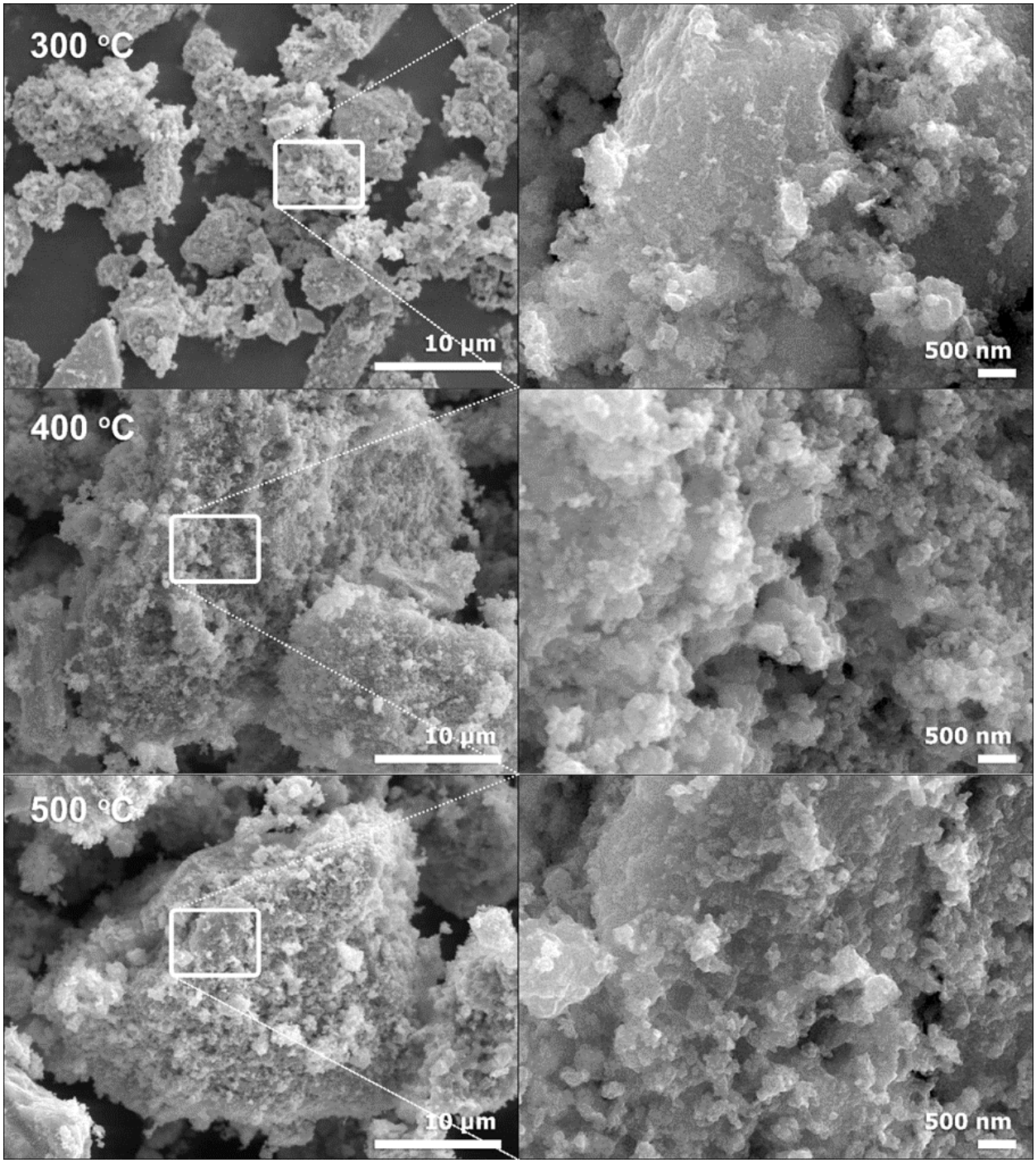

Figure 2: Microstructural evolution of SnO_2 nanoparticles with calcination temperature. SEM micrographs at low and high magnification show morphology and agglomeration at 300°C, 400°C, and 500°C.

Image analysis was conducted using MountainsMap software by measuring over 100 particles from the SEM micrographs. This quantitative analysis reaffirmed the particle enlargement at higher calcination temperatures.

The sintering led to a reduction in porosity and surface area. The particle growth likely occurs due to accumulation, interparticle fusion, and Ostwald ripening effects, which are accelerated at elevated temperatures [33]. The SEM findings corroborate well with the crystallite growth inferred from XRD peak narrowing. The smaller particle size and higher specific surface area of the 300°C sample would facilitate increased surface redox reactions. In contrast, the surface available for catalytic antibacterial activity may be restricted in the larger particles of the 400°C and 500°C samples. Thus, SEM provided critical insights into the surface morphology, microstructure evolution, and sintering dynamics of nanocrystalline SnO_2 particles with the variation in thermal processing conditions. The EDS spectra in Fig. 3 confirm the presence of tin (Sn) and oxygen (O) as the predominant elements in all three SnO_2 samples calcined at 300°C, 400°C, and 500°C. This verifies the chemical composition aligns with pure SnO_2, as expected from the synthesis method. Additionally, residual traces of chlorine (Cl) originating from the tin chloride precursor are observed. The Cl content declines from 0.9 wt% in the 300°C sample to 0.21 wt% in the 500°C sample. The reduction of Cl impurity with higher calcination temperature indicates a more thorough removal of remnant precursor and improved sample purity. Estimating the atomic Sn/O ratios from the EDS data reveals values approaching the ideal stoichiometric ratio of 0.5 for SnO_2 across all samples. The proximity of measured Sn/O ratios to 0.5 confirms the precipitation and calcination approach yields near-stoichiometric SnO_2 nanoparticles without substantial oxygen vacancies. In summary, the EDS elemental analysis verifies the successful synthesis of stoichiometric SnO_2 nanopowder after calcination, with systematic decreases in residual Cl impurities at higher temperatures. The results validate the phase purity and composition of the SnO_2 nanoparticles obtained through the low-cost, eco-friendly chemical precipitation route.

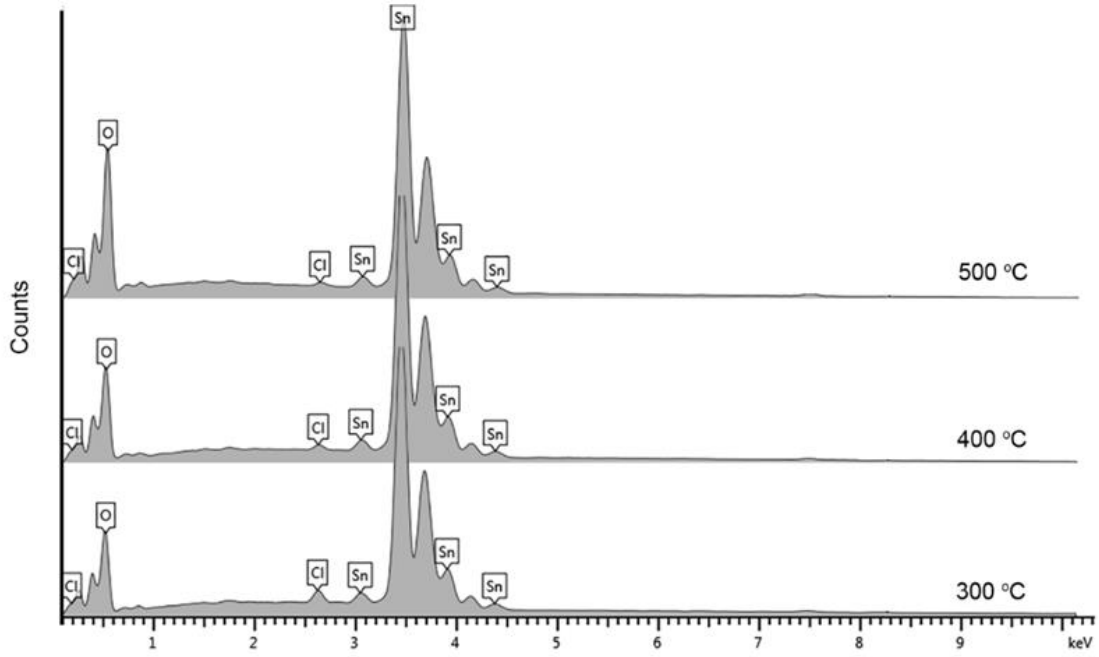

Figure 3: Elemental analysis of SnO_2 nanoparticles by EDS. Spectra for the samples calcined at 300°C, 400°C and 500°C confirm the presence of Sn and O as major elements and trace Cl.

Fourier transform infrared (FTIR) spectroscopy elucidated the progression of chemical bonding configurations and vibrational fingerprints in the as-synthesized and calcined SnO_2 nanoparticles (Fig. 4). The precursor sample heated to 100°C exhibited a broad envelope centred at 3348 cm^{-1} attributed to the O-H stretching vibrations of absorbed water molecules and N-H stretching of ammonium residues from the synthesis [34, 35]. The peaks at 1606 cm-1, 714 cm^{-1} and 537 cm^{-1} are ascribed to the H-O-H bending, Sn-O stretching, and Sn-Cl stretching modes respectively [36, 37]. The emergence of these bands corroborates the formation of a hydrated oxyhydroxide intermediate phase along with unreacted tin chloride precursor, as inferred from XRD patterns. Upon calcination to 300°C, the O-H and N-H peaks diminished, indicating desorption of physisorbed species. Simultaneously, new asymmetric CO_2 stretches manifested at 2341 cm^{-1} and 2360 cm^{-1} due to atmospheric carbon dioxide. The broad envelope spanning 500-850 cm^{-1} originates from overlapped metal-oxygen lattice vibrations of nanocrystalline

SnO_2. The intense peak at 608 cm-1, accompanied by a shoulder around 459 $cm^{-1,}$ represents the asymmetric and symmetric O-Sn-O bridging stretches, respectively [31, 35, 38]. The surface Sn-O-Sn bending mode contributes to the band at 855 cm^{-1} [36, 39]. With increasing calcination temperature to 400°C and 500°C, incremental blue-shifting and sharpening of these Sn-O-Sn and O-Sn-O peaks occurred, congruent with improved crystallinity and particle growth as evidenced in XRD and SEM. Concurrently, the Sn-Cl stretching mode at 537 cm^{-1} faded and disappeared by 300°C, indicative of complete hydrolysis of tin chloride to stoichiometric SnO_2, further validated by declining chlorine content in EDS analysis. The FTIR analysis substantiated the chemical pathway involving thermal desorption of precursor species and crystallization of nanocrystalline SnO_2 exhibiting characteristic vibrational fingerprints. The trends align well with phase evolution observed using diffraction and microscopy techniques.

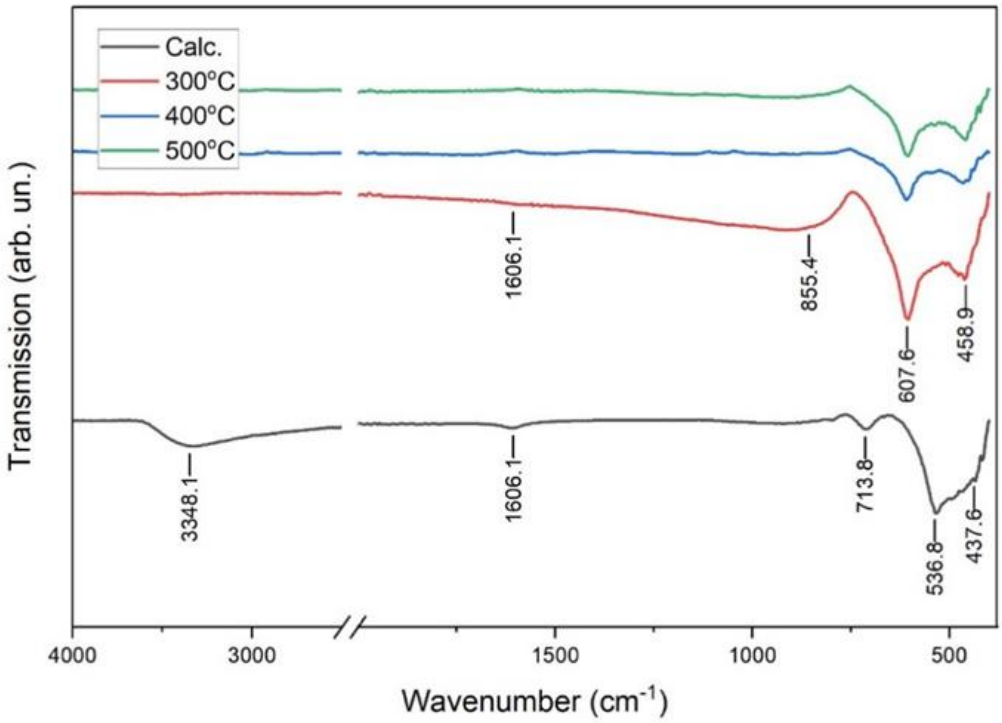

Figure 4: Calcination-induced changes in FTIR spectra of SnO_2. Broad envelope from 500-700 cm^{-1} represents Sn-O-Sn and O-Sn-O vibrational fingerprints in samples treated at 100°C, 300°C, 400°C and 500°C.

3.2 Antibacterial Performance

The antibacterial activity of the SnO_2 nanoparticles calcined at 300°C, 400°C and 500°C was evaluated against model Gram-negative *E. coli* and Gram-positive *S. aureus* bacterial strains using standard agar well diffusion assays [40, 41]. As seen in the zone of inhibition (ZOI) results (Fig. 5), the SnO_2 nanoparticles exhibited excellent antibacterial power against *E. coli* and *S. aureus*, as evident from the clear ZOIs formed around the nanoparticle-loaded wells. The extent of ZOI gave a quantitative indication of the antibacterial activity. Interestingly, an inverse correlation between the SnO_2 crystallite size and antibacterial activity was observed. The 300°C calcined sample with the smallest crystallite size of 11.9 nm showed maximum inhibition zone diameters of 25 mm and 29 mm for *E. coli* and *S. aureus*, respectively. The enhanced antibacterial effect of the lower crystallite size SnO_2 sample is attributed to the higher surface area and increased density of surface defects such as oxygen vacancies. This can promote the generation of reactive oxygen species (ROS) like •OH, $O_2^{-\bullet}$ and H_2O_2 when the particles are irradiated or upon interaction with bacterial cells. ROS can damage the cell membrane and intracellular components, leading to leakage of cytoplasmic content and cell death. Additional mechanisms involve direct oxidative damage of cell wall/membrane by SnO_2 nanoparticle interaction and release of Sn^{2+} ions.

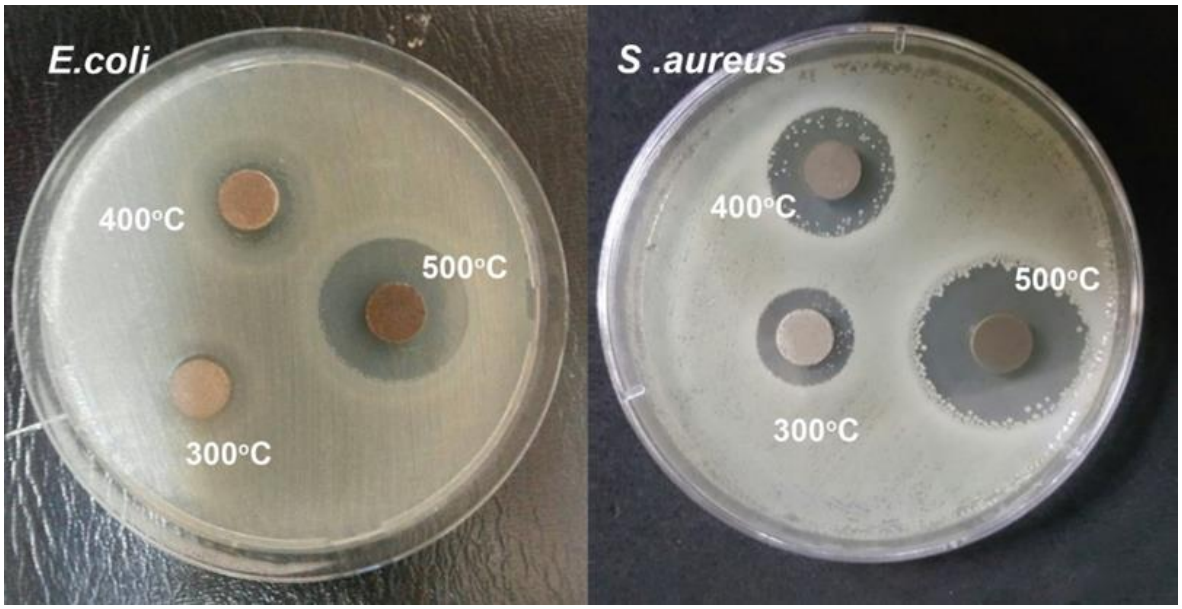

Figure 5: Photographs showing antibacterial activity of SnO_2 nanoparticles calcined at different temperatures against *E. coli* and *S. aureus* by zone of inhibition method.

Another factor is the cell wall structure of the bacterial strains. The thicker peptidoglycan layer of Gram-positive *S. aureus* could be more prone to ROS attack compared to the lipopolysaccharide membrane of Gram-negative *E. coli*. The results demonstrate that the SnO_2 nanoparticle crystallite size can be effectively tailored by tuning the calcination temperature to achieve optimal antibacterial activity against both Gram-types of pathogenic bacteria. The data in Table 2 shows the relationship between the crystallite size of calcined SnO_2 nanoparticles and their antibacterial activity against *E. coli* and *S. aureus*, as measured by inhibition zone diameter. As the calcination temperature was increased from 300°C to 500°C, the crystallite size of the SnO_2 nanoparticles systematically grew larger, from 11.9 nm to 17.2 nm, due to sintering and particle growth effects.

Table 2: Correlation between crystallite size of calcined SnO_2 nanoparticles and inhibition zone diameter for *E. coli* and *S. aureus* bacterial strains.

Calcinations Temperature OC	Crystallite Size (nm)	ZOI (mm) *E. coli*	ZOI (mm) *S. aureus*
300	11.93	25	29
400	13.87	13	22
500	17.21	11	17

Correspondingly, the inhibition zone diameters for both bacterial strains consistently decreased with increasing SnO_2 crystallite size. The sample calcined at 300°C, with the smallest crystallite size of 11.9 nm, exhibited the most significant inhibition zones of 25 mm for *E. coli* and 29 mm for *S. aureus*. In contrast, the sample calcined at 500°C, with the largest crystallite size of 17.2 nm, showed the narrowest inhibition zones of 11 mm for *E. coli* and 17 mm for S. aureus. This inverse relationship demonstrates that the antibacterial activity is reduced as the crystallite size of the SnO_2 nanoparticles increases. The enhanced antibacterial activity of smaller SnO_2 crystallites can be attributed to their larger surface area and higher density of surface defects, which can more effectively generate reactive oxygen species. Table 3 compiles the antibacterial activity of SnO_2 nanoparticles synthesized by various methods reported in literature against different microorganisms. It can be observed that the precipitation-synthesized SnO_2 NPs in this work exhibit comparable or superior antibacterial activity relative to SnO_2 prepared by other more complex techniques. The SnO_2 NPs synthesized via precipitation in this study showed a zone of inhibition ranging from 11-29 mm against *E. coli* and *S. aureus*. This activity is similar to SnO_2 NPs of comparable size prepared by co-precipitation (10-22 mm ZOI) [25, 26], precipitation (6-15 mm ZOI) [30], sol-gel (2-18 mm ZOI) [18] and other methods (8-24 mm ZOI) [27–29, 31]. The excellent antibacterial performance of the precipitated SnO_2 NPs demonstrates that high crystallinity and appropriate nanoparticle size are more critical

factors than the synthesis technique. The precipitation method produces high-purity crystalline SnO_2 NPs of suitable size to penetrate bacteria cells and generate ROS to damage cellular components. The table highlights the potential of these facile precipitation-synthesized SnO_2 NPs as antibacterial agents against both Gram-positive and Gram-negative pathogenic bacteria.

Table 3: Comparison of antibacterial activity (zone of inhibition, ZOI) of SnO_2 nanoparticles.

Synthesis Method	Composition	Crystallite Size (nm)	Microorganism	ZOI (mm)	Ref.
Co-precipitation	SnO_2, CuO doped SnO_2	10-15	E-coli K-neumo S-aureus	10	[25]
Co-precipitation	SnO_2, Co doped SnO_2	24.8	E-coli B-subtilis	16-22	[26]
Precipitation	SnO_2	NPs	E-coli S-aureus	6-15	[30]
Sol-Gel	SnO_2	9-10	E-coli Micrococcus luteus	2-18	[18]
Precipitation	SnO_2	18.79	E-coli B-subtilis Pseudomonas aeruginosa	8-12	[31]
Biosynthesis	SnO_2	35	E-coli B-subtilis S-aureus Pseudomonas aeruginosa	16-24	[28]
Biosynthesis	SnO_2	18.2	E-coli B-subtilis S-aureus S. pyogenes K. pneumoniae	9-15	[29]
Ultra-sonochemical	SnO_2	5-30	E-coli C. albicans	14-22	[27]
Precipitation	SnO_2	12-17	E-coli S-aureus	11-29	Current work

5. Conclusions

In this work, SnO_2 nanoparticles were successfully synthesized via a simple chemical precipitation route using tin chloride and ammonia precursors at room temperature. XRD studies confirmed the formation of tetragonal SnO_2 with high phase purity after calcination from 300°C to 500°C. The average crystallite size systematically increased from 11.9 nm to 17.2 nm with higher calcination temperature due to sintering. FTIR spectra revealed the characteristic Sn-O and O-Sn-O vibrational modes in the samples. SEM micrographs demonstrated the particle size enlargement from ~68 nm to ~93 nm upon calcining from 300°C to 500°C due to aggregation and Ostwald ripening effects. The antibacterial activity of the calcined SnO_2 nanoparticles against *E. coli* and *S. aureus* was found to be inversely related to the crystallite size. The sample calcined at a lower temperature of 300°C with the smallest crystallite size of 11.9 nm exhibited maximum inhibition zones of 25 mm and 29 mm against *E. coli* and *S. aureus*, respectively. The higher surface area and surface defects in smaller crystallites can generate reactive oxygen species, thereby enhancing antibacterial behaviour. This work demonstrates that the SnO_2 nanoparticle crystallinity and morphology can be effectively tailored by tuning the calcination temperature to achieve optimal antibacterial action against Gram-positive and Gram-negative pathogenic bacteria. The green chemistry approach presents a facile route for controlling the antibacterial activity of SnO_2 nanomaterials for water treatment and food packaging applications.

Acknowledgement
The authors thank the Center of Advanced Materials at the Materials Research Directorate for supporting this work. The facilities and resources have been invaluable, allowing us to synthesize and characterize the SnO_2 nanoparticles.

Conflict of Interest
The authors declare that they have no conflict of interest.

References
[1] Das, S., and Jayaraman, V. "SnO2: A Comprehensive Review on Structures and Gas Sensors." *Progress in Materials Science*, vol. 66, 2014, pp. 112–255.

[2] Ismail, R. A., Erten-Ela, S., Ali, A. K., Yavuz, C., and Hassoon, K. I. "Pulsed Laser Ablation of Tin Oxide Nanoparticles in Liquid for Optoelectronic Devices." *Silicon*, vol. 13, no. 9, 2021, pp. 3229–3237.

[3] Bhawna, Choudhary, A. K., Gupta, A., Kumar, S., Kumar, P., Singh, R. P., Singh, P., and Kumar, V. "Synthesis, Antimicrobial Activity, and Photocatalytic Performance of Ce Doped SnO2 Nanoparticles." *Frontiers in Nanotechnology*, vol. 2, vo. vember, volume 2, 2020, pp. 1–7.

[4] Kamble, D. L., Harale, N. S., Patil, V. L., Patil, P. S., and Kadam, L. D. "Characterization and NO_2 Gas Sensing Properties of Spray Pyrolyzed SnO2 Thin Films." *Journal of Analytical and Applied Pyrolysis*, vol. 127, no. 2, 2017, pp. 38–46.

[5] Zarkov, A., Stanulis, A., Mikoliunaite, L., Salak, A. N., and Kareiva, A. "Organic-Free Synthesis of Nanostructured SnO_2 Thin Films by Chemical Solution Deposition." *Thin Solid Films*, vol. 649, 2018, pp. 219–224.

[6] Abdelkrim, A., Rahmane, S., Abdelouahab, O., Abdelmalek, N., and Brahim, G. "Effect of Solution Concentration on the Structural, Optical and Electrical Properties of SnO2 Thin Films Prepared by Spray Pyrolysis." *Optik*, vol. 127, no. 5, 2016, pp. 2653–2658.

[7] Abdulsattar, M. A., Batros, S. S., and Addie, A. J. "Indium Doped SnO2nanostructures Preparation and Properties Supported by DFT Study." *Superlattices and Microstructures*, vol. 100, 2016, pp. 342–349.

[8] Hassan, A. I., Addie, A. J., and Admon, J. "Influence of Precursor Concentration on the Optoelectronic Properties of Spray Deposited SnO 2 /Si Heterojunction." *Materials Research Express*, vol. 6, no. 9, 2019, p. 0950c4.

[9] Chowdhury, F. R., Choudhury, S., Hasan, F., and Begum, T. "Optical Properties of Undoped and Indium-Doped Tin Oxide Thin Films." *Journal of Bangladesh Academy of Sciences*, vol. 35, no. 1, 2013, pp. 99–111.

[10] Ji, Z., He, Z., Song, Y., Liu, K., and Ye, Z. "Fabrication and Characterization of Indium-Doped p-Type SnO2 Thin Films." *Journal of Crystal Growth*, vol. 259, no. 3, 2003, pp. 282–285.

[11] Li, Z., Shen, W., Zhang, X., Fang, L., and Zu, X. "Controllable Growth of SnO_2 Nanoparticles by Citric Acid Assisted Hydrothermal Process." *Colloids and Surfaces A: Physicochemical and Engineering Aspects*, vol. 327, Nos. 1–3, 2008, pp. 17–20.

[12] Drzymała, E., Gruzeł, G., Depciuch, J., Budziak, A., Kowal, A., and Parlinska-Wojtan, M. "Structural, Chemical and Optical Properties of SnO 2 NPs Obtained by Three Different Synthesis Routes." *Journal of Physics and Chemistry of Solids*, vol. 107, 2017, pp. 100–107.

[13] T. Lamdhade, G., C. Raghuwanshi, F., M. Agrawal, R., M. Balkhande, V., and Shripath, T. "SnO2 Nanoparticles Synthesis Via Liquid-Phase Co-Precipitation Technique." *Advanced Materials Letters*, vol. 6, no. 8, 2015, pp. 738–742.

[14] Chen, W., Ghosh, D., and Chen, S. "Large-Scale Electrochemical Synthesis of SnO2 Nanoparticles." *Journal of Materials Science*, vol. 43, no. 15, 2008, pp. 5291–5299.

[15] Ravichandran, K., Shalini, R., Ayyanar, M., Kavitha, P., Baneto, M., Karunakaran, M., Praseetha, P. K., Pushpa, K. C. S., and Anuradha, N. "Effect of PH of the Precursor Solution on the Photocatalytic and Biomedical Applications of Enzyme Coupled ZnO and SnO2 Nanomaterials: A Comparative Study." *Journal of Water Process Engineering*, vol. 53, no. May, 2023, p. 103817.

[16] Zhang, Q., Zou, X., Wang, Y., and Habibi, M. "Study on Photocatalytic, Electric, and Sensing Behavior of Co- and Ag-Codoped Tin Dioxide (SnO2) Nano Particles." *Materials Science and Engineering: B*, vol. 296, no. April, 2023, p. 116687.

[17] Batzill, M., and Diebold, U. "The Surface and Materials Science of Tin Oxide." *Progress in Surface Science*, vol. 79, Nos. 2–4, 2005, pp. 47–154.

[18] Bilal Ahmad, T., Asif, A. B., Atif Khurshid, W., Masood, A. K., and Gulzar Ahmad, S. "Preparation and Characterization of SnO2 Nanoparticles for Antibacterial Properties." *Nanomaterial Chemistry and Technology*, vol. 2, no. 1, 2020, pp. 1–5.

[19] Yuliarto, B., Gumilar, G., Zulhendri, D. W., Nugraha, and Septiani, N. L. W. "Preparation of SnO2 Thin Film Nanostructure for CO Gas Sensor Using Ultrasonic Spray Pyrolysis and Chemical Bath Deposition Technique." *Acta Physica Polonica A*, vol. 131, no. 3, 2017, pp. 534–538.

[20] Galal, A., Hassan, H. K., Atta, N. F., Abdel-Mageed, A. M., and Jacob, T. "Synthesis, Structural and Morphological Characterizations of Nano-Ru-Based Perovskites/RGO Composites." *Scientific Reports*, vol. 9, no. 1, 2019, pp. 1–13.

[21] Meena Kumari, M., and Philip, D. "Synthesis of Biogenic SnO2 Nanoparticles and Evaluation of Thermal, Rheological, Antibacterial and Antioxidant Activities." *Powder Technology*, vol. 270, 2015, pp. 312–319.

[22] Samrot, A. V., Sahithya, C. S., Selvarani A, J., Purayil, S. K., and Ponnaiah, P. "A Review on Synthesis, Characterization and Potential Biological Applications of Superparamagnetic Iron Oxide Nanoparticles." *Current Research in Green and Sustainable Chemistry*, vol. 4, no. December 2020, 2021, p. 100042.

[23] Amininezhad, S. M., Rezvani, A., Amouheidari, M., Amininejad, S. M., and Rakhshani, S. "The Antibacterial Activity of SnO2 Nanoparticles against Escherichia Coli and Staphylococcus Aureus." *Zahedan Journal of Research in Medical Sciences*, vol. 17, no. 9, 2015.

[24] Cavaliere, E., De Cesari, S., Landini, G., Riccobono, E., Pallecchi, L., Rossolini, G. M., and Gavioli, L. "Highly Bactericidal Ag Nanoparticle Films Obtained by Cluster Beam Deposition." *Nanomedicine: Nanotechnology, Biology, and Medicine*, vol. 11, no. 6, 2015, pp. 1417–1423.

[25] Gopal, S., Iruson, B., Balaraman, S., Krishnmoorthy, S., and Elayaperumal, M. "Effect on Optical and Antibacterial Activity of SnO2 and CuO Blended SnO2 Nanoparticles." *Soft Nanoscience Letters*, vol. 13, no. 02, 2023, pp. 1–12.

[26] Qamar, M., Shahid, S., Khan, S. A., Zaman, S., and Sarwar, M. N. "SYNTHESIS CHARACTERIZATION , OPTICAL AND ANTIBACTERIAL STUDIES OF Co-DOPED SnO 2 NANOPARTICLES." *Digest*

Journal of Nanomaterials and Biostructures, vol. 12, no. 4, 2017, pp. 1127–1135.

[27] Rehman, S., Asiri, S. M., Khan, F. A., Jermy, B. R., Khan, H., Akhtar, S., Jindan, R. Al, Khan, K. M., and Qurashi, A. "Biocompatible Tin Oxide Nanoparticles: Synthesis, Antibacterial, Anticandidal and Cytotoxic Activities." *ChemistrySelect*, vol. 4, no. 14, 2019, pp. 4013–4017.

[28] Al-Enazi, N. M., Ameen, F., Alsamhary, K., Dawoud, T., Al-Khattaf, F., and AlNadhari, S. "Tin Oxide Nanoparticles (SnO2-NPs) Synthesis Using Galaxaura Elongata and Its Anti-Microbial and Cytotoxicity Study: A Greenery Approach." *Applied Nanoscience (Switzerland)*, vol. 13, no. 1, 2023, pp. 519–527.

[29] Fatimah, I., Purwiandono, G., Hidayat, H., Sagadevan, S., Ghazali, S. A. I. S. M., Oh, W. C., and Doong, R. A. "Flower-like Sno2 Nanoparticle Biofabrication Using Pometia Pinnata Leaf Extract and Study on Its Photocatalytic and Antibacterial Activities." *Nanomaterials*, vol. 11, no. 11, 2021.

[30] Khanoma, R., Parveenb, S., and Hasan, M. "Antimicrobial Activity of SnO 2 Nanoparticles against Escherichia Coli and Staphylococcus Aureus and Conventional Antibiotics." *American Scientific Research Journal for Engineering, Technology, and Sciences*, vol. 46, no. 1, 2018, pp. 111–121.

[31] Abirami, S., Viruthagiri, G., and Ashokkumar, K. "Structural, Morphological and Anti - Bacterial Activities of Pure SnO2 Nanoparticles Prepared by Chemical Precipitation Method." *Materials Today: Proceedings*, Vol. 73, 2023, pp. 535–538.

[32] Abdulsattar, M. A., Batros, S. S., and Addie, A. J. "Spectroscopic Properties of Indium-Doped CdO Nanostructures Supported by DFT Calculations." *Surface Review and Letters*, vol. 26, no. 04, 2019, p. 1850169.

[33] Palasantzas, G., Vystavel, T., Koch, S. A., and De Hosson, J. T. M. "Coalescence Aspects of Cobalt Nanoparticles during in Situ High-Temperature Annealing." *Journal of Applied Physics*, vol. 99, no. 2, 2006.

[34] Orel, B., Lavrenčič-Štankgar, U., Crnjak-Orel, Z., Bukovec, P., and Kosec, M. "Structural and FTIR Spectroscopic Studies of Gel-Xerogel-Oxide Transitions of SnO 2 and SnO 2 : Sb Powders and Dip-Coated Films Prepared via Inorganic Sol-Gel Route." *Journal of Non-Crystalline Solids*, vol. 167, no. 3, 1994, pp. 272–288.

[35] Mahmood, H., Khan, M. A., Mohuddin, B., and Iqbal, T. "Solution-Phase Growth of Tin Oxide (SnO2) Nanostructures: Structural, Optical and Photocatalytic Properties." *Materials Science and Engineering B: Solid-State Materials for Advanced Technology*, vol. 258, no. August 2018, 2020, p. 114568.

[36] Sukriti, and Chand, P. "Effect of PH Values on the Structural, Optical and Electrical Properties of SnO2 Nanostructures." *Optik*, vol. 181, no. September 2018, 2019, pp. 768–778.

[37] Keny, S. J., Srivastava, A. P., Debnath, A. K., Adhikari, S., and Rath, M. C. "One-Step Synthesis of Tin Oxide Nanoparticles in Aqueous Solution Induced by Free Radicals." *Materials Chemistry and Physics*, vol. 286, o. December 2021, 2022, p. 126184.

[38] Perumal, V., Inmozhi, C., Uthrakumar, R., Robert, R., Chandrasekar, M., Mohamed, S. B., Honey, S., Raja, A., Al-Mekhlafi, F. A., and Kaviyarasu, K. "Enhancing the Photocatalytic Performance of Surface - Treated SnO2 Hierarchical Nanorods against Methylene Blue Dye under Solar Irradiation and Biological Degradation." *Environmental Research*, vol. 209, no. September 2021, 2022, p. 112821.

[39] Yakout, S. M. "Engineering of Visible Light Photocatalytic Activity in SnO2 Nanoparticles: Cu2+-Integrated Li+, Y3+ or Zr4+ Dopants." *Optical Materials*, vol. 116, no. April, 2021, p. 111077.

[40] Hikmet, R., and Hussein, N. "The Biological Activity of Mycosynthesized Silver Nanoparticles Against Some Pathogenic Bacteria." *Journal of Applied Sciences and Nanotechnology*, vol. 2, no. 1, 2022, pp. 59–68.

[41] Khedaer, Z., Ahmed, D., and Al-Jawad, S. "Investigation of Morphological, Optical, and Antibacterial Properties of Hybrid ZnO-MWCNT Prepared by Sol-Gel." *Journal of Applied Sciences and Nanotechnology*, vol. 1, no. 2, 2021, pp. 66–77.